Prediction of Glioma Stemlike Cell Infiltration in the Non–Contrast-Enhancing Area by Quantitative Measurement of Lactate on Magnetic Resonance Spectroscopy in Glioblastoma

Q1 Q8 Q9 Q10 Q7 *Akihiro Inoue[1], Masahiro Nishikawa[1], Takanori Ohnishi[2], Hajime Yano[3], Yonehiro Kanemura[4,5], Yoshihiro Ohtsuka[1], Saya Ozaki[1], Yawara Nakamura[1], Shirabe Matsumoto[1], Satoshi Suehiro[1], Daisuke Yamashita[1], Seiji Shigekawa[1], Hideaki Watanabe[1], Riko Kitazawa[6], Junya Tanaka[3], Takeharu Kunieda[1]*

BACKGROUND: **We previously reported that glioma stemlike cells (GSCs) exist in the area of the tumor periphery showing no gadolinium enhancement on magnetic resonance imaging. In the present work, we analyzed glucose metabolism to investigate whether lactate could be predictive of tumor invasiveness and of use in detection of the tumor invasion area in glioblastoma multiforme (GBM).**

METHODS: **The expression of lactate dehydrogenase A (*LDH-A*) and pyruvate dehydrogenase (*PDH*) was investigated in 20 patients. In GSC lines, *LDH-A* and *PDH* expression also was examined in parallel to assessments of mitochondrial respiration. We then investigated the relationship between lactate/creatine ratios in the tumor periphery measured by magnetic resonance spectroscopy, using learning-compression-model algorithms and phenotypes of GBMs.**

RESULTS: **In 20 GBMs, high-invasive GBM expressed *LDH-A* at significantly higher expression than did low-invasive GBM, whereas low-invasive GBM showed significantly higher expression of *PDH* than did high-invasive GBM. The highly invasive GSC line showed higher expression of *LDH-A* and lower expression of *PDH* compared with low-invasive GSC lines. The highly invasive GSC line also showed the lowest consumption of oxygen and the lowest production of adenosine triphosphate.**

Key words
- CD44
- Glioblastoma
- Glucose metabolism
- Lactate
- LC-Model algorithm
- Magnetic resonance spectroscopy

Abbreviations and Acronyms
ATP: Adenosine triphosphate
CD: Cluster of differentiation
Cr: Creatine
ETR: Extensive total resection
FLAIR: Fluid-attenuated inversion recovery
GBM: Glioblastoma multiforme
Gd: Gadolinium
Gln: Glutamine
GSC: Glioma stemlike cell
GTR: Gross total resection
HI: Highly invasive
HIF-1: Hypoxia-inducible factor 1
Lac: Lactate
LC: Learning-Compression
LDH-A: Lactate dehydrogenase A
LI: Low-invasive
Met: Methionine
MGMT: O(6)-methylguanine-DNA methyltransferase
MRI: Magnetic resonance imaging
mRNA: Messenger RNA
MRS: Magnetic resonance spectroscopy
NAA: *N*-acetyl-aspartate
OCR: Oxygen consumption rate
OS: Overall survival
PDH: Pyruvate dehydrogenase
PET: Positron emission tomography
PFS: Progression-free survival
qRT-PCR: Quantitative real-time reverse transcription-polymerase chain reaction
RF: Radiofrequency
SUV_{max}: Maximum standard uptake value
TCA: Tricarboxylic acid
TNR: Tumor/contralateral normal brain tissue ratio
WI: Weighted image

From the [1]Department of Neurosurgery, Ehime University School of Medicine, Toon, Ehime; [2]Department of Neurosurgery, Washoukai Sadamoto Hospital, Matsuyama, Ehime; [3]Department of Molecular and Cellular Physiology, Ehime University School of Medicine, Toon, Ehime; Departments of [4]Biomedical Research and Innovation, Institute for Clinical Research and [5]Neurosurgery, National Hospital Organization Osaka National Hospital, Osaka, Japan; and [6]Division of Diagnostic Pathology, Ehime University Hospital, Toon, Ehime, Japan

To whom correspondence should be addressed: Akihiro Inoue, M.D., Ph.D. [E-mail: iakihiro3@gmail.com]

Citation: World Neurosurg. (2021). https://doi.org/10.1016/j.wneu.2021.06.044

*Journal homepage: **www.journals.elsevier.com/world-neurosurgery***

*Available online: **www.sciencedirect.com***

FLA 5.6.0 DTD ■ WNEU17386_proof ■ 2 July 2021 ■ 8:36 pm ■ ce

Lactate levels, as measured by magnetic resonance spectroscopy, showed a significant positive correlation with *LDH-A* transcript levels, permitting classification of the GBMs into high-invasive and low-invasive phenotypes based on a cutoff value of 0.66 in the lactate/creatine ratio.

CONCLUSIONS: **In the tumor periphery area of the highly invasive GBM, aerobic glycolysis was the predominant pathway for glucose metabolism, resulting in the accumulation of lactate. The level of lactate may facilitate prediction of the tumor-infiltrating area on GBM.**

INTRODUCTION

Glioblastoma multiforme (GBM) is the most malignant primary brain tumor, with the poor prognosis of a median survival of 15 months after maximum resection of the tumor followed by the standard radiochemotherapy.[1,2] The poor prognosis of GBM is largely caused by glioma stemlike cells (GSCs), which characteristically show highly invasive (HI) and migratory activities. Recurrence of GBM likely occurs from GSCs that survive tumor resection and radiochemotherapy. In previous work, we showed that GSCs are present in the tumor periphery of HI-type GBM. We showed this fact by establishing HI GSC lines through the primary culture of tumor cells from the periphery of GBM tumors that show a higher level of expression of cluster of differentiation (CD) 44 in the periphery than in the core.[3] Consequently, to improve the prognosis of GBM (particularly the HI type of GBM), it is important to identify, using contrast enhancement, and resect the GSCs that have infiltrated the non−contrast-enhancing area around the GBM tumor mass.[3]

As ^{11}C methionine (Met)−positron emission tomography (PET) studies have shown, the area of tumor extension of GBM, including infiltrating tumors, is generally wider than the gadolinium (Gd)-enhanced tumor area on magnetic resonance imaging (MRI).[4,5] The higher the tumor invasiveness, the wider the tumor-infiltrating area showing no Gd enhancement.[6] Consequently, to perform the maximum resection of tumors, including infiltrating tumor cells in GBM, it is critical to evaluate how far the tumor invasion has extended and where the HI tumor cells, including GSCs, are located. We reported a HI type of GBM that expresses CD44 at a high level in the tumor periphery; patients with GBM of this type showed earlier tumor progression and worse survival compared with a low-invasive (LI)/proliferative type of GBM with low expression of CD44.[3] Consequently, CD44 expression in the tumor tissues is believed to be a useful marker to predict invasiveness and prognosis of GBMs. However, this marker is of no use before surgery because its evaluation requires resected tumor tissues. Here, we focus on energy metabolism by GBM, which uses 2 distinct pathways for glucose metabolism: aerobic glycolysis and oxidation via tricarboxylic acid (TCA) cycle (using mitochondrial functions). Of the two, aerobic glycolysis is a major pathway to produce energy and reduced nicotinamide adenine dinucleotide in cancer cells (Warburg effect); the final product of aerobic glycolysis is lactate (Lac), which acidifies the microenvironment, thereby facilitating tumor invasion.[7,8] Accordingly, the more Lac that is produced, the higher the tumor invasiveness. On the other hand, various types of cells are present in the peritumoral edematous area of GBM, including neurons, glial cells, macrophages, and microglia. Among these cells, neurons and astrocytes are known to function synergistically to achieve effective energy metabolism.[9] The effects of such neurometabolic coupling on Lac production should be considered to allow exact evaluation of Lac levels in the tumor periphery. Astrocytes also metabolize glucose to Lac via aerobic glycolysis. The Lac produced is released and transferred via monocarboxylate transporters to neurons, where it is converted to pyruvate to allow the generation of adenosine triphosphate (ATP) via oxidative phosphorylation through the TCA cycle (the astrocyte-to-neuron Lac shuttle hypothesis).[10,11] If neurons are injured and lose their activity, extracellular Lac levels may be further increased, resulting in enhancement of the acidity of the microenvironment at the periphery of GBM.

In the present study, we analyzed whether invasive phenotypes of GBM correlate with the pattern of glucose metabolic pathway use. In addition, we investigated whether Lac/creatine (Cr) values, assessed using magnetic resonance spectroscopy (MRS) with Learning-Compression (LC) Model postprocessing, might be a marker for preoperative evaluation of the phenotypic type of GBM and prediction of the non−contrast-enhancing tumor-infiltrating area (including GSCs) beyond the contrast-enhancing tumor mass of GBM on MRI.[12-14]

METHODS

All procedures performed in studies involving human participants were in accordance with the ethical standards of the institutional and/or national research committee and with the Helsinki Declaration and its later amendments or comparable ethical standards. The present study was approved by the local ethics committee for clinical research of Ehime University School of Medicine, and informed consent was obtained from each individual patient.

Patients and Study Design

This study enrolled 20 patients whose tumors were verified histologically as GBM; all were being treated at the Department of Neurosurgery of Ehime University Hospital, between July 2018 and December 2020, according to a uniform treatment protocol. Informed consent was obtained from all individual participants enrolled in the study; the participants were informed regarding the risk of the surgical procedure and the potential risks of microsurgery and chemoradiotherapy. All patients underwent craniotomy for tumor resection, followed by radiotherapy (60 Gy) and chemotherapy with temozolomide in accordance with the Stupp protocol.[1] Tumor samples were obtained from 2 different sites (the tumor core and the tumor periphery) using navigation-guided microsurgical techniques as described previously.[15] Details of the procedure for taking tissue samples are presented in **Supplementary Figure 1**.

The tumor samples were frozen and preserved at −80°C until use. Total RNA, prepared from the tumor samples from the 20 patients with GBM, was used for quantitative real-time reverse

FLA 5.6.0 DTD ■ WNEU17386_proof ■ 2 July 2021 ■ 8:36 pm ■ ce

transcription-polymerase chain reaction (qRT-PCR). The qRT-PCR measured the messenger RNA (mRNA) expression of genes encoding Lac dehydrogenase A (*LDH-A*) and pyruvate dehydrogenase (*PDH*) (to analyze the glycolytic metabolism) as well as that of the gene encoding the GBM stem cell marker CD44. In addition, using human GSC lines, we examined the transcriptional expression of the genes encoding *LDH-A* and *PDH* and also analyzed the oxygen consumption rate (OCR) of these lines using an XFp Extracellular Flux Analyzer (Agilent Seahorse Bioscience, Santa Clara, California, USA) to measure mitochondrial energy metabolism. We investigated possible relationships between Lac levels, as measured by MRS, and the expression of *CD44*, in both the tumor periphery and the tumor core. The resulting ratios between values in the tumor periphery and tumor core (P/C ratios) were used to assess whether the measurement of Lac by MRS facilitated prediction of the tumor phenotypes and prognoses of the patients with GBM.

MRI and Met-PET

All patients had MRI studies to clarify the nature, location, and size of the GBM tumors, as well as the associated degree of brain edema. Most cases of GBM can be divided into 2 phenotypes (HI and LI types) based on the results of MRI as aided by Met-PET.[3,6,16] MRI was performed using a 3-T scanner (Achieva [Philips, Best, The Netherlands]) with a standard coil. Axial, coronal, and sagittal T1-weighted images (WI) were obtained with slice thickness of 2 mm before and after intravenous administration of Gd–diethylene triamine pentaacetate (0.1 mmol/kg). T2-WI with the 3 directions and axial images of fluid-attenuated inversion recovery (FLAIR) also were obtained. PET studies were performed in three-dimensional acquisition mode. Images were acquired while patients rested in the supine position with their eyes closed. ^{11}C-Met-PET data were acquired for 20 minutes, beginning at 20 minutes after the administration of a Met dose of 5 MBq/kg body weight. The maximum standard uptake value (SUV_{max}) of each tumor was calculated by obtaining the pixel values of a region of interest placed on the tumor image with reference to the Gd-enhanced T1WI. The tumor/contralateral normal brain tissue ratio (TNR) was determined by dividing the tumor SUV_{max} by the mean standard uptake value of the contralateral occipital lobe.

GSC Culture

Three human GSC lines (GSL-HI, GSL-LI, and GDC40) were used in the present study. The first 2 GSC lines, GSL-HI and GSL-LI, were established previously from the primary cell culture of tissues surgically obtained from the tumor periphery of patients with GBM.[3] The third GSC line, GDC40, was established in Osaka National Hospital (Osaka, Japan).[17] These GSC lines were cultured in neural stem cell medium, which consisted of serum-free Dulbecco's modified eagle medium/Ham's F-12 medium (Wako) containing 10 μg/mL insulin (Wako), 10 nmol/L recombinant human basic fibroblast growth factor, 10 nmol/L recombinant human epidermal growth factor, 5 μmol/L heparin, N2 supplement (Wako), GlutaMAX supplement (Gibco), and penicillin/streptomycin/amphotericin B mixture. Growth factors were purchased from PeproTech (London, United Kingdom). The stemness of these GSC lines was confirmed by evaluating their sphere-forming ability before starting each set of studies.

RNA Isolation and qRT-PCR

Total RNA was extracted from the tissue of each tumor sample (both core and periphery) and from cells of each GSC line using ISOGEN (Nippon Gene, Tokyo, Japan) according to the manufacturer's instructions. Complementary DNA was synthesized using ReverTra Ace qPCR RT Master Mix with a gDNA remover kit (Toyobo). qPCR analysis was performed using Fast Start Universal SYBR Green Master Mix (Roche Diagnostic Japan) with an MJ Mini instrument (BioRad, Hercules, California, USA). All gene-specific mRNA expression values were normalized relative to the expression level of *GAPDH* (glyceraldehyde-3-phosphate dehydrogenase), a housekeeping (reference) gene encoding glyceraldehyde-3-phosphate dehydrogenase. Quantification of gene expression was performed using ΔCt values, wherein ΔCt is defined as the difference between the target and reference gene Ct values. All primer sequences are listed in **Supplementary Table 1**.

Measurement of Mitochondrial Energy Metabolism in GSCs

To evaluate mitochondrial energy metabolism, the OCR was measured in each of the 3 GSC lines using an XFp Extracellular Flux Analyzer.[18,19] GSCs were seeded in E2 in 8-well plates (provided by the flux analyzer manufacturer) at 2.5×10^4 cells/well. Two of the 8 wells of each plate were used as blanks. After overnight incubation in a CO_2 incubator, the plates were placed in the XFp analyzer, which was operated according to the manufacturer's instructions. Specifically, oligomycin A (1.0 μM), FCCP (carbonyl cyanide 4 (trifluoromethoxy) phenylhydrazone; 1 μM), rotenone (0.5 μM), and antimycin A (0.5 μM) were automatically and sequentially added to the cells to determine the rates of basal respiration, maximal respiration, and ATP production, which are known mitochondrial activities.

MRS in Patients with GBM

Within 1 week before surgery, all patients underwent preoperative MRI and MRS. A 3-T MRI/MRS scanner (General Electric Healthcare, Waukesha, Wisconsin, USA) was used to acquire the magnetic resonance spectral data. A 48-channel head MRI coil was used for receiving the signal, and the quadrature body MRI coil was used for transmitting the radiofrequency (RF) pulses. Single-voxel localized magnetic resonance spectra were acquired using the double-echo point-resolved spectroscopy sequence.[20] Voxels were localized to representative areas of solid tumor, as determined by a board-certified neuroradiologist. Regions of probable necrosis, hemorrhage, or cystic changes, if present, were excluded from the interrogated area. As a control, voxels also were placed in the same anatomic location on the contralateral (nontumor) side of the brain to obtain control spectra. The MRS acquisition parameters were as follows: $2 \times 2 \times 2$ cm^3 and repetition time/echo time = 2 seconds/35 milliseconds, with 128 averages and 2048 complex points for the spectral data. Water enhanced through T1-based global presuppression of water was achieved using 3 frequency-selective RF pulses; each RF pulse was followed by dephasing Bo-crusher gradient pulses.[21] Unsuppressed water signal also was acquired using the same parameters as above, except with only 4 averages. Patient spectra were assessed for artifacts and signal/noise ratio. Spectra with the full width at half maximum of N-acetyl-aspartate (NAA) of >30 Hz or poor water suppression were excluded based on these objective criteria.

LC-Model Algorithm

After recording the MRS, we processed the raw data files using the LC-Model algorithm.[22] The LC-Model processing was performed in exactly the same way for each spectrum, with no changes in preprocessing or modifications to the control file. The water-suppressed spectral domain data were analyzed across the range of 0.5–4.0 ppm. Using the GAMMA library,[23] the basis set for 2-hydroxyglutarate was developed, assuming a pH value of 7.0. In addition, the basis set provided by the vendor was used and then scaled to a consistent transmitter gain. Assuming a water concentration of 35 M (15), absolute values of 2-hydroxyglutarate, glutamate, glutamine (Gln), choline, Cr, NAA, Lac, and other metabolites were reported in mM per kg of wet tissue uncorrected for T1 and T2 saturation. Using the LC-Model, both ratios of metabolites (with respect to total Cr concentration) and absolute concentrations of metabolites (using known concentrations of tissue water) can be calculated.[22] The target area for the LC-Model algorithm was set to the Met-uptake area at TNR 1.4, which corresponded to the non–contrast-enhancing area around the main tumor with Gd enhancement. Any 3 points were selected in the area, and amounts of various molecules were measured by the LC-Model algorithm. The concentration (resonance area ratio; mmol/L) of each molecule was measured, and the calculated concentration of Lac was presented as a Lac/Cr ratio, in units of relative mmol/L (when Cr is set to 1.0) (**Figure 1**).

Statistical Analysis

Values were expressed as the mean ± standard deviation, and the data were compared using a 2-tailed Student *t* test (unpaired). Comparisons among >2 groups were conducted using 2-tailed 1-way analysis of variance with the Tukey post hoc test. Kaplan-Meier plots were generated to estimate unadjusted time-to-event variables. Spearman correlation analysis was performed to examine correlations for nonparametric data. Significance was set at $P < 0.05$. All analyses were performed using Office Excel 2016 software (Microsoft, Redmond, Washington, USA) and Easy R (EZR) free software version 1.54 (Saitama Medical Center, Jichi Medical University, Saitama, Japan).[24]

RESULTS

Patient Characteristics

We treated 33 patients with GBM at our institution during the research period. Among these patients, 20 for whom both MRI and MRS analysis could be performed were enrolled in this research. All patients received image-guided microsurgical resection followed by chemotherapy and radiation therapy.[25] Histopathologic evaluation verified that all tumors were GBM, as judged by the World Health Organization classification system, and that all tumors lacked a mutation in the gene encoding *IDH-1* (isocitrate dehydrogenase 1). The presence of hotspot mutations in *IDH1* (R132) was analyzed by Sanger sequencing. Expression of O(6)- methylguanine-DNA methyltransferase (MGMT) and the Ki-67 staining index in the core of the tumors are summarized in **Table 1**. The methylation status of the *MGMT* promoter was analyzed by quantitative methylation-specific PCR after bisulfate modification of genomic DNA, and we used a cutoff of ≥1% for *MGMT* promoter methylation.[26] The mean age of the 20 patients was 65.35 years (range, 19–85 years) with 14 men and 6 women; the patients presented with a median Karnofsky Performance Status of 80 (range, 40–100). The mean of body mass index (calculated as weight in kilograms divided by the square of height in meters) was 21.0 (range, 14.5–25.9). These characteristics of patients are summarized in **Table 1**. None of the characteristics significantly correlated with patients' survival. In addition, various adjuvant therapies, including bis-chloroethyl nitrosourea (BCNU) wafer, Novo TTF (tumor treating field) and bevacizumab, were given to the patients, as shown in **Table 1**. However, there was no correlation between these adjuvant therapies and patients' survival. The extent of resection was evaluated by volumetric analysis on MRI before and after surgery, as described previously.[25] Gross total resection (GTR: 100% resection of the tumor volume), subtotal resection (95%–100% resection), and partial resection (<95% resection) were achieved in 11 patients (55.0%), 1 patient (5.0%), and 8 patients (40.0%), respectively. Among patients with GTR, 8 received extensive resection of a part of infiltrating tumors in the non–contrast-enhancing area around Gd-enhanced tumor mass with the aid of a fluorescence guide of 5-aminolevulinic acid (extensive total resection [ETR]) (**Table 1**). The progression-free survival (PFS) and overall survival (OS) of these patients are presented in **Table 1**. The survival curves of OS and PFS, excluding 2 patients (numbers 19 and 20) who remained alive without tumor progression and whose follow-up time was very short, of the remaining 18 patients and 7 patients who received ETR are presented in **Supplementary Figure 2**. The median PFS and OS of all 18 patients were 10.85 and 20.7 months, respectively. In contrast, those of 7 patients with ETR were 15.9 and 31.6 months, respectively.

Classification by MRI of Phenotypes in Twenty GBMs

As we described in a previous report, most GBMs can be classified as either of 2 phenotypes, HI and LI types, according to the criteria of the imaging features on MRI aided by PET imaging.[6,16] The criteria were defined as follows. The HI phenotype of GBM includes an irregular margin with heterogeneously and not intensely enhanced wall by the contrast, diffuse edema surrounding the tumor, and an area of contrast-enhancing tumor that is smaller than the area of Met uptake at TNR 1.4. In contrast, the criteria for the less (low)-invasive phenotype of GBM consist of a relatively well-demarcated margin with intensely enhanced wall or homogeneously enhanced solid mass, focal (not extensive) edema, and an area of contrast-enhancing tumor that is almost the same as or slightly smaller than the area of Met uptake at TNR 1.4. The representative imaging features on MRI and Met-PET of the 2 phenotypes and criteria of the phenotypes are presented in **Figure 2**. The results for the 20 patients with GBM are summarized in **Table 2**. Of the 20 patients with GBM examined in the present study, 11 showed a HI phenotype and 9 patients presented with a LI phenotype.

Expression of Genes Encoding the Stem Cell Marker CD44 and Subunits of the Enzymes Related to Glucose Metabolism (LDH-A and PDH)

We measured the mRNA expression of the gene encoding the stem cell marker CD44 in the tumor core and periphery, and calculated the ratio of amounts of CD44 expression in the tumor periphery to those in the tumor core (P/C ratio) in 20 patients with

FLA 5.6.0 DTD ■ WNEU17386_proof ■ 2 July 2021 ■ 8:36 pm ■ ce

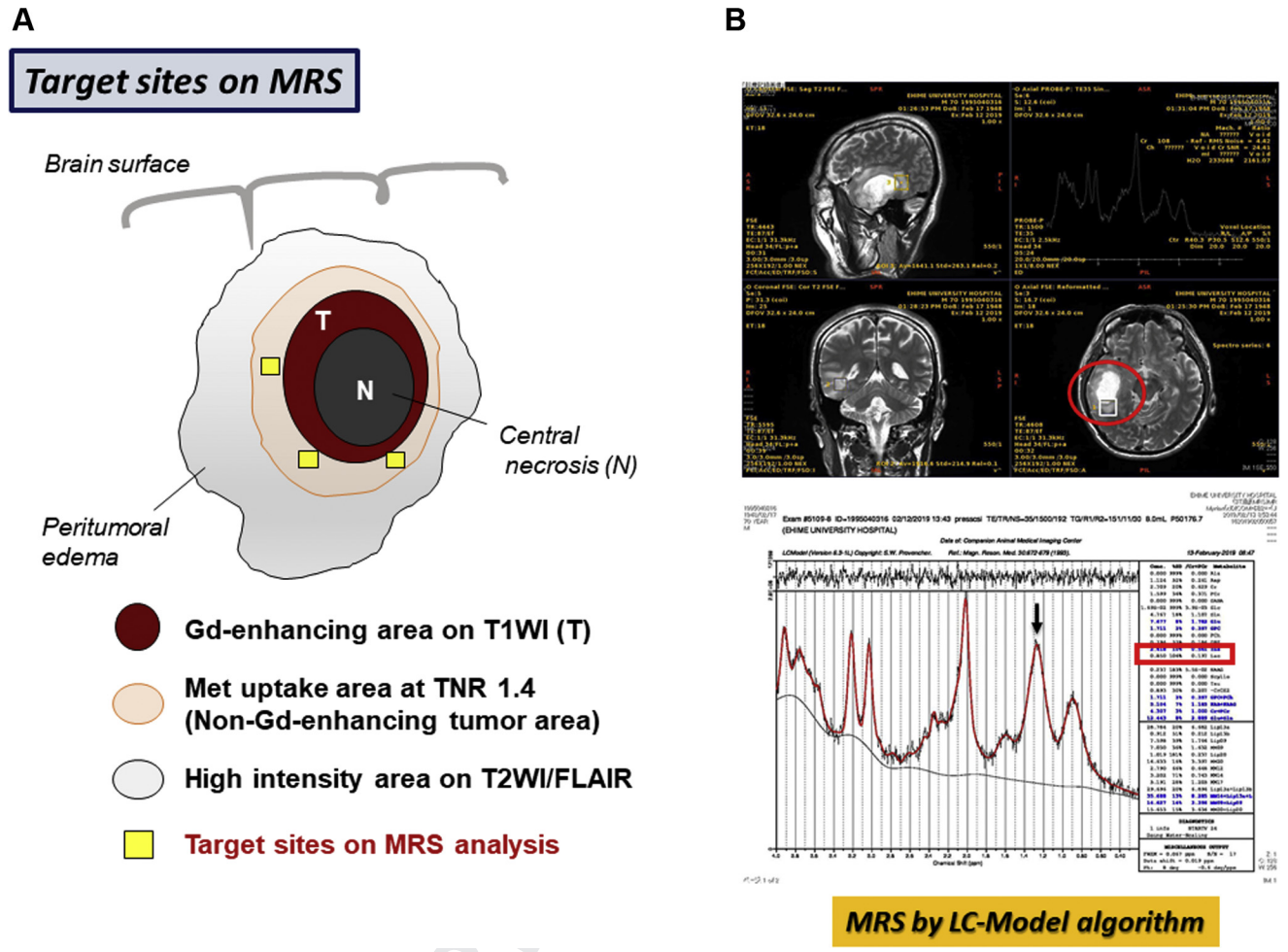

Figure 1. Magnetic resonance spectroscopy (MRS) in patients with glioblastoma (GBM). (**A**) Target sites on MRS. Magnetic resonance spectral data were obtained at the following site: the ^{11}C-methionine uptake area (possessing a tumor/contralateral normal brain tissue ratio (TNR) of 1.4) in the high intensity area on fluid-attenuated inversion recovery (FLAIR)/magnetic resonance imaging and slightly outside the gadolinium (Gd) contrast range of T1-weighted imaging (T1WI)/magnetic resonance imaging. Any 3 points were extracted from this region. (**B**) Results of quantitative analysis of metabolites by Learning-Compression (LC) Model (*red circle*, target site). The waveform of the MRS is shown on the left side (*black arrow*, lactate), and the metabolites analyzed quantitatively are shown on the right side. The content is expressed in absolute value. The value of lactate is boxed with a *red square*. T2WI, T2-weighted imaging.

GBM. In addition, we analyzed expression of the genes encoding subunits of 2 enzymes (*LDH-A* and *PDH*) representative of glucose metabolism by aerobic glycolysis and the TCA cycle, respectively (Figure 3A) (Table 2). We confirmed that the mean value of the P/C ratio of *CD44* expression in the HI-type GBM was significantly higher than that in the LI-type GBM (HI, 9.89 ± 4.37 (mean ± standard deviation); LI, 1.97 ± 1.96; $P = 0.000091$) (Figure 3B). Expression of *LDH-A* showed a significant positive correlation with the P/C ratio of *CD44* expression ($R = 0.596$; $P = 0.0056$), whereas expression of *PDH* showed a significant negative correlation with the P/C ratio of *CD44* expression ($R = -0.734$; $P = 0.00035$) (Figure 3C). In addition, HI-type GBM showed significantly higher *LDHA* transcript levels than did LI-type GBM (HI, 9.399 ± 1.138; LI, 1.311 ± 0.650; $P < 0.00001$) (Figure 3D). In contrast, LI-type GBM accumulated significantly higher amounts of *PDH* mRNA than did HI-type GBM (LI, 7.06 ± 3.00; HI, 3.24 ± 1.32; $P = 0.0013$) (Figure 3E).

Expression of LDH-A and PDH, and Mitochondrial OCRs in GSCs

We investigated expression of *LDH-A* and *PDH* in 3 GSC lines and also tested these lines for mitochondrial energy metabolism by means of the Seahorse Mito-Stress Test using an XFp Extracellular Flux Analyzer, which assesses OCR. The HI GSC-HI line, which had higher *CD44* expression, showed the highest expression of *LDH-A* and the lowest expression of *PDH*, whereas GDC40, which had the lowest invasiveness of the 3 cell lines, showed the lower

FLA 5.6.0 DTD ■ WNEU17386_proof ■ 2 July 2021 ■ 8:36 pm ■ ce

Table 1. Patient Characteristics Including Surgical Results and Outcome

Patient Number	Age (Years)	Sex	Body Mass Index (kg/m^2)	Karnofsky Performance Status (%)	Tumor Location	O(6)-Methylguanine-DNA Methyltransferase (m)	Ki-67 Labeling Index (%)	Extent of Resection	Adjuvant Medication: Bis-Chloroethyl Nitrosourea Wafer	Adjuvant Medication: *Novo* Tumor Treating Field	Adjuvant Medication: Bevacizumab	Survival: Progression-Free Survival (Months)	Survival: Overall Survival (Months)	Outcome
1	60	M	22.2	70	Lt. parietal	−	40	PR	−	−	+	3.7	20.5	D
2	74	M	24.1	90	Lt. temporal	+	50	GTR (E)	+	−	+	15.9	20.7	D
3	64	M	24.3	70	Rt. parietal	−	25	PR	+	−	+	2.9	14.2	D
4	63	F	23.3	60	Rt. frontal	+	50	GTR (E)	+	−	+	24.1	31.6	D
5	76	M	22.8	90	Rt. posterior	−	15	GTR	+	−	+	6.4	18.6	D
6	52	F	21.2	70	Lt. parietal	+	40	GTR (E)	+	−	+	8.5	38.5+	A
7	85	M	17.5	80	Rt. posterior	+	40	GTR (E)	−	−	−	32.9+	32.9+	A
8	53	M	22.2	80	Rt. posterior	+	30	GTR	+	−	+	2.1	13.1	D
9	64	M	20.2	70	Lt. temporal	+	40	GTR	+	−	+	7.3	16.3	D
10	72	M	22.2	90	Rt. temporal	−	30	GTR (E)	+	+	+	15.7	26.5+	A
11	19	M	22.1	60	Bilateral frontal	−	60	PR	−	−	+	16	16	D
12	79	F	25.9	60	Rt. thalamus	−	10	PR	−	−	+	1.3	25.0+	A
13	58	F	19.1	90	Rt. parietal	−	40	GTR (E)	+	+	+	13.2	21.5	D
14	73	M	15.5	80	Lt. frontal	+	20	PR	+	−	−	8.5	8.5	D
15	76	F	14.5	90	Lt. frontal	+	25	PR	−	−	−	20.6+	20.6+	A
16	37	M	21.8	90	Lt. parietal	−	55	PR	+	+	+	1.4	17.9+	A

FLA 5.6.0 DTD ■ WNEU17386_proof ■ 2 July 2021 ■ 8:36 pm ■ ce

17	80	M	23.6	100	Rt. parietal	–	15	GTR (E)	+	–	14.6+	A
18	76	M	24.1	40	Rt. frontal	+	40	PR	–	–	10.6+	A
19	75	M	18.4	60	Rt. temporal	+	50	GTR (E)	+	–	7.5+	A
20	71	F	15.8	90	Rt. temporal	+	20	Subtotal resection	+	–	3.7+	A

M, male; Lt, left; PR, partial resection; D, dead; GTR (E), gross total resection with extensive resection of the infiltrating tumors; Rt, right; F, female; GTR, gross total resection; A, alive; NA, not assessed.

expression of both *CD44* and *LDH-A* and the highest expression of *PDH* (Figure 4A). On the other hand, measurement of OCR permitted determination of basal and maximal respiration, and of the levels of ATP production, in the GSCs. All 3 parameters of mitochondrial metabolism were higher in GSC-LI and GDC40 than in GSC-HI (Figure 4B).

MRS Analysis Using the LC-Model Algorithm

MRS analysis with the LC-Model algorithm was performed on all 20 patients. Lac was obtained as a waveform on the MRS at approximately 1.33 ppm in all analyses, and the values of Lac/Cr ratio in all 20 patients are shown in Table 2. Spearman correlation analysis showed that the values of Lac/Cr ratio by MRS had a significant positive correlation with the expression levels of *LDHA* ($R = 0.589$; $P = 0.0063$) (Figure 5A, *left*). Expression levels of *PDH* and the Lac/Cr ratio seemed to show a negative correlation, but this effect fell short of significance (Figure 5A, *right*). The values of the Lac/Cr ratio showed a significant positive correlation with the values of the P/C ratio of *CD44* expression (Figure 5B). In addition, HI-type GBMs had significantly higher values of Lac/Cr ratio than did LI-type GBMs (HI, 1.339 ± 0.4866; LI, 0.386 ± 0.140; $P = 0.000023$) (Figure 5C). The cutoff value of Lac/Cr ratio for HI-type GBM was >0.66 (sensitivity, 100%; specificity, 90.9%). We present 2 representative cases in the following sections.

Illustrative Cases

Case 1 (Presented Patient 2). A 74-year-old man was admitted to our hospital with a chronic headache that had gradually worsened over the preceding month. Neurologic examination showed right-sided quadrant hemianopsia. Gd-enhanced MRI showed a homogeneously enhanced tumor in the left temporal lobe and perifocal hyperintensity on FLAIR (Figure 6A and B). A PET scan of the brain showed strongly increased uptake of Met in the left temporal lobe, consistent with the lesion seen by MRI (SUV_{max} for Met [T/N ratio], 4.38) (Figure 6C). The accumulation area of Met was largely consistent with the Gd-enhanced lesion in the MRI. Based on the preoperative diagnosis of LI-type GBM, tumor resection was performed by craniotomy with the assistance of image-guided navigation by MRI (reference for T1WI after administration of Gd) and Met-PET imaging (GTR with extensive resection). Histopathologic examination of the surgical specimen from the Gd-enhanced lesion showed a typical pathologic pattern of GBM; the Ki-67 proliferation-related labeling index was 50.0%. The P/C ratio of *CD44* mRNA expression was 0.33. MRS analysis using the LC-Model algorithm provided an Lac/Cr ratio of 0.18 in the Met accumulation sites, with TNR 1.4 outside the Gd contrast area on MRI (Figure 6D).

Case 2 (Presented Patient 1). A 60-year-old man visited our department after experiencing partial epilepsy. On admission, he presented with numbness of the right extremities. Gd-enhanced MRI showed several heterogeneously enhanced tumors and extended hyperintensities around the several enhanced tumors on FLAIR in the left frontal lobe (Figure 7A and B). A PET scan showed highly increased uptake of Met, larger uptake area compared with the lesion seen by MRI (SUV_{max} values for Met,

FLA 5.6.0 DTD ■ WNEU17386_proof ■ 2 July 2021 ■ 8:36 pm ■ ce

5.21) (Figure 7C). Based on these tests, the tumor was believed to be a HI GBM, and craniotomy was performed with the assistance of image-guided navigation by MRI and Met-PET imaging (partial resection). Postoperative histopathology confirmed that the tumor was a GBM; immunohistochemical examination disclosed a high Ki-67 labeling index (40.0%). The P/C ratio for *CD44* transcript levels was 8.21. MRS using the LC-Model algorithm showed an Lac/Cr value of 2.01 in the Met accumulation sites, with TNR 1.4 outside the Gd contrast area by MRI (Figure 7D).

DISCUSSION

Malignant gliomas, in particular GBMs, are HI brain tumors, and it is difficult to show the entire tumor including infiltrating tumor cells on anatomic imaging modalities such as computed tomography and MRI.[1-3] Met-PET has been shown to be a useful imaging modality for more accurate delineation of the extent of tumor invasion from solid GBM masses.[6] In our previous study, we reported that the area of ^{11}C-Met uptake at a TNR of 1.4 in PET images of GBMs was generally larger than the area of Gd-enhanced tumor mass by MRI. In addition, in the area showing Met uptake of TNR 1.4 outside the Gd-enhanced tumor mass, immunohistochemical analysis showed the presence of CD133- and nestin-double-positive GSCs.[6] Consequently, this area may be regarded as an invasion niche whose hypoxic microenvironment provides favorable conditions for GSCs to maintain their stemness.

Clinically, it has been reported that supratotal resection of GBM including such non–contrast-enhancing tumors presented prognostic benefits over those obtained by GTR of the contrast-enhancing tumor alone.[27,28] Also, in the present study, ETR including partial removal of the infiltrating tumors beyond Gd-enhanced tumor mass showed longer median OS (31.6 months) compared with the median OS (20.5 months) in GTR with resection of Gd-enhanced tumor alone using the same navigation system in our previous study.[29] Although Met-PET is useful as an imaging modality in the diagnosis and treatment of malignant brain tumors, the instrument is not universally available, given the high cost of both installing PET-computed tomography and cyclotron and performing the examination. To identify the non–contrast-enhancing tumor in the tumor periphery beyond the border of contrast-enhancing tumor component, MRI has usually

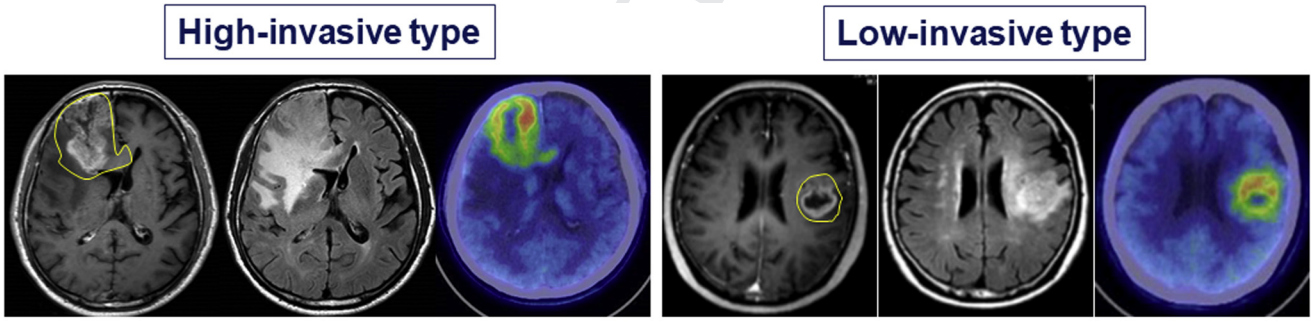

Criteria of invasiveness phenotypes of GBM on MRI and Met-PET

Features on MRI/Met-PET	High-invasive	Low-invasive
1. Tumor margin	irregular	demarcated
2. Enhancement of margin wall	weak~moderate/ heterogeneous	intense/ homogeneous
3. Peritumoral edema	diffuse	focal
4. Area of Gd+ vs Met-PET (TNR 1.4)	Gd << Met-PET	Gd ≤ Met-PET

Figure 2. Imaging phenotype on magnetic resonance imaging in 20 glioblastomas (GBMs). From characteristic features of GBM on magnetic resonance imaging (MRI) and ^{11}C-methionine (Met)-positron emission tomography (PET) imaging analysis, 20 patients were classified as having a highly invasive or a low-invasive/demarcated phenotype. Representative images of the 2 phenotypes are shown in the *upper panel*. *Yellow circle lines* drawn around the gadolinium (Gd)-enhanced tumor on the Gd-T1 weighted image (T1) represent the border of the Met-uptake area at a tumor/contralateral normal brain tissue ratio (TNR) of 1.4. Eleven patients showed the high-invasive-type of tumor, and the remaining 9 patients presented with a low-invasive and relatively well-demarcated type of tumor. The criteria of the GBM phenotypes are presented in the *lower panel*. FLAIR, fluid-attenuated inversion recovery.

FLA 5.6.0 DTD ■ WNEU17386_proof ■ 2 July 2021 ■ 8:36 pm ■ ce

Table 2. Summary of CD44, Lactate Dehydrogenase A, Pyruvate Dehydrogenase, and Lactate/Creatine Expression Values and Features on Magnetic Resonance Imaging in 20 Patients with Glioblastoma Multiforme

Patient Number	CD44		Periphery/Core Ratio (CD44)	Lactate Dehydrogenase A (Periphery)	Pyruvate Dehydrogenase (Periphery)	Lactate/Cr Value	*N*-Acetyl-Aspartate/Cr Value	Glutamate/Cr Value	Glutamine/Cr Value	Magnetic Resonance Imaging Invasiveness
	Core	Periphery								
1	7.2	59.1	8.21	8.03	5.47	2.01	0.26	1.11	1.25	High
2	1.2	0.4	0.33	2.16	10.39	0.18	1.2	1.33	0.76	Low
3	0.3	2.4	8.05	10.8	3.46	1.61	0.59	0.3	0.83	High
4	4.9	40.8	8.38	10	4.31	1.87	0.48	0.42	0.65	High
5	0.3	0.04	0.15	2.19	10.83	0.33	1.06	1.26	0.95	Low
6	1.6	0.04	0.02	1.16	8.39	0.32	1.12	0.84	1.25	Low
7	1.5	7.1	4.71	1.03	3.48	0.52	0.95	1.05	1.1	Low
8	2.2	11.6	5.38	1.03	5.32	0.37	1.17	0.93	1.03	Low
9	3.3	31.1	9.38	9.03	4.82	1.24	0.63	0.43	0.87	High
10	1	2.4	1.19	0.03	2.5	0.32	1.38	1.78	1.11	Low
11	20.9	18	0.86	9.34	3.51	0.22	0.16	0.94	0.69	High
12	0.3	0.3	1.06	1.27	8.93	0.66	1.14	1.23	1.17	Low
13	1.2	2.9	2.55	1.54	5.51	0.32	1.35	1.15	1.17	Low
14	3.2	41.7	13.08	11.29	2.36	1.02	0.59	0.84	0.4	High
15	1.3	13.1	9.84	9.03	1.31	1.7	1.4	1.62	1.11	High
16	1.6	16.2	10.32	7.65	1.39	1.2	0.75	1.41	1.73	High
17	0.3	0.6	2.37	1.39	8.37	0.45	1.02	1.08	0.91	Low
18	4.9	59.9	12.24	8.43	2.37	1.13	0.65	0.98	0.53	High
19	1.2	22.8	19.1	9.44	3.3	1.38	0.55	0.85	0.64	High
20	2	18.6	9.31	10.35	3.56	1.35	0.48	0.89	0.66	High

Cr, creatine.

FLA 5.6.0 DTD ■ WNEU17386_proof ■ 2 July 2021 ■ 8:36 pm ■ ce

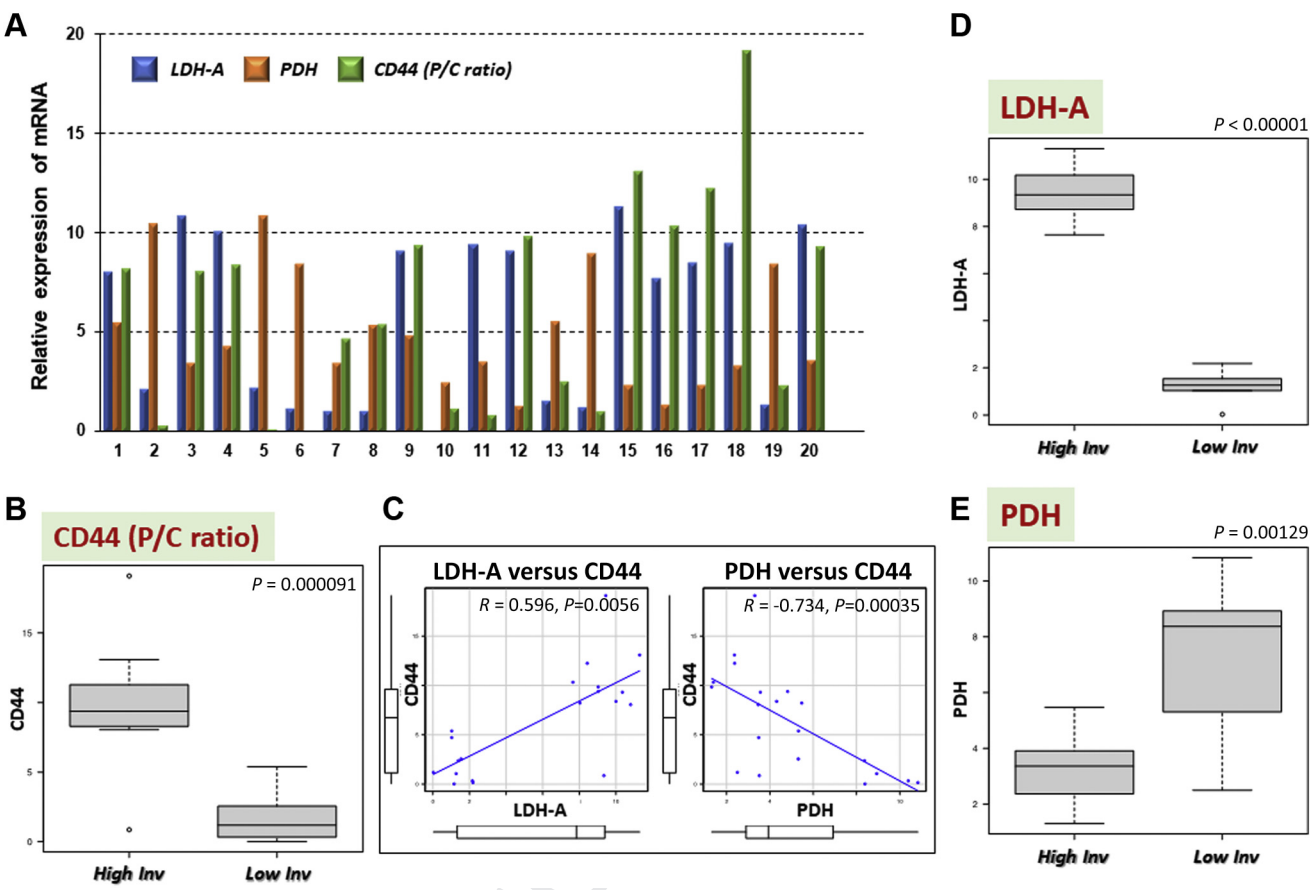

Figure 3. Expressions and relations of genes encoding key enzymes in glucose metabolism and CD44. (**A**) Messenger RNA (mRNA) expression of the genes encoding subunits of lactate dehydrogenase A (*LDH-A*) and pyruvate dehydrogenase (*PDH*) in the tumor periphery, and periphery/core (P/C) ratio of *CD44* expression in 20 patients with glioblastoma (GBM). The values of expression of *LDH-A* and *PDH* are for relative mRNA expression (normalized to that of the housekeeping gene *GAPDH*). The P/C ratio is the ratio of *CD44* transcript level in the tumor periphery to that in the tumor core. (**B**) Highly invasive (inv) GBMs exhibited *CD44* P/C ratios that were significantly higher level than those of low-invasive GBMs ($P = 0.000091$). (**C**) The P/C ratios for *LDH-A* and *CD44* expression showed a significant positive correlation ($R = 0.596$; $P = 0.0056$), whereas those of *PDH* and *CD44* showed a significant negative correlation ($R = -0.734$; $P = 0.00035$). (**D** and **E**) Highly invasive GBMs showed significantly higher *LDH-A* expression than did low-invasive GBMs ($P < 0.00001$). Low-invasive GBMs showed significantly higher *PDH* expression than did highly invasive GBMs ($P = 00129$).

been applied by combining Gd-enhanced T1WIs and FLAIR sequence images.[27,30] These MRI techniques facilitate the differentiation of non−contrast-enhancing tumor tissue from vasogenic edema, permitting identification of non−contrast-enhancing tumor tissue in GBM.[31] However, it is not clear whether the non−contrast-enhancing tumor tissue identified by such MRI include the GSCs that are believed to be responsible for tumor recurrence in GBM. Accordingly, development of a new method to evaluate the area of infiltrating tumors in the tumor periphery of GBM is desirable for eradicating GBM. To establish a safe and simple diagnostic modality replacing Met-PET, we focused on glucose metabolism in GBM and analyzed the metabolic pathways in the tumor periphery outside the Gd-enhanced tumor mass, a region in which infiltrating GSCs may be present. The GSCs that exist in the tumor periphery of HI GBM are believed to be exposed to a hypoxic microenvironment, given that this area is accompanied by diffuse peritumoral edema and lacks neovasculature. Therefore, the GSCs are expected to use primarily aerobic glycolysis for glucose metabolism, in the same way that other cancer cells do. The fate of pyruvate produced by glycolysis is determined by 2 key enzymes the activities of which depend on oxygen availability. In normal cells, in the presence of oxygen, pyruvate is transferred into the mitochondria and converted into acetyl-coenzyme A by PDH; the acetyl-coenzyme A then is used for oxidation of glucose via the TCA cycle. In contrast, in cancer cells in which the microenvironment is typically hypoxic, the pyruvate is converted into Lac by LDH-A (Warburg effect).[7,8] The expression of LDH-A is activated by hypoxia-inducible

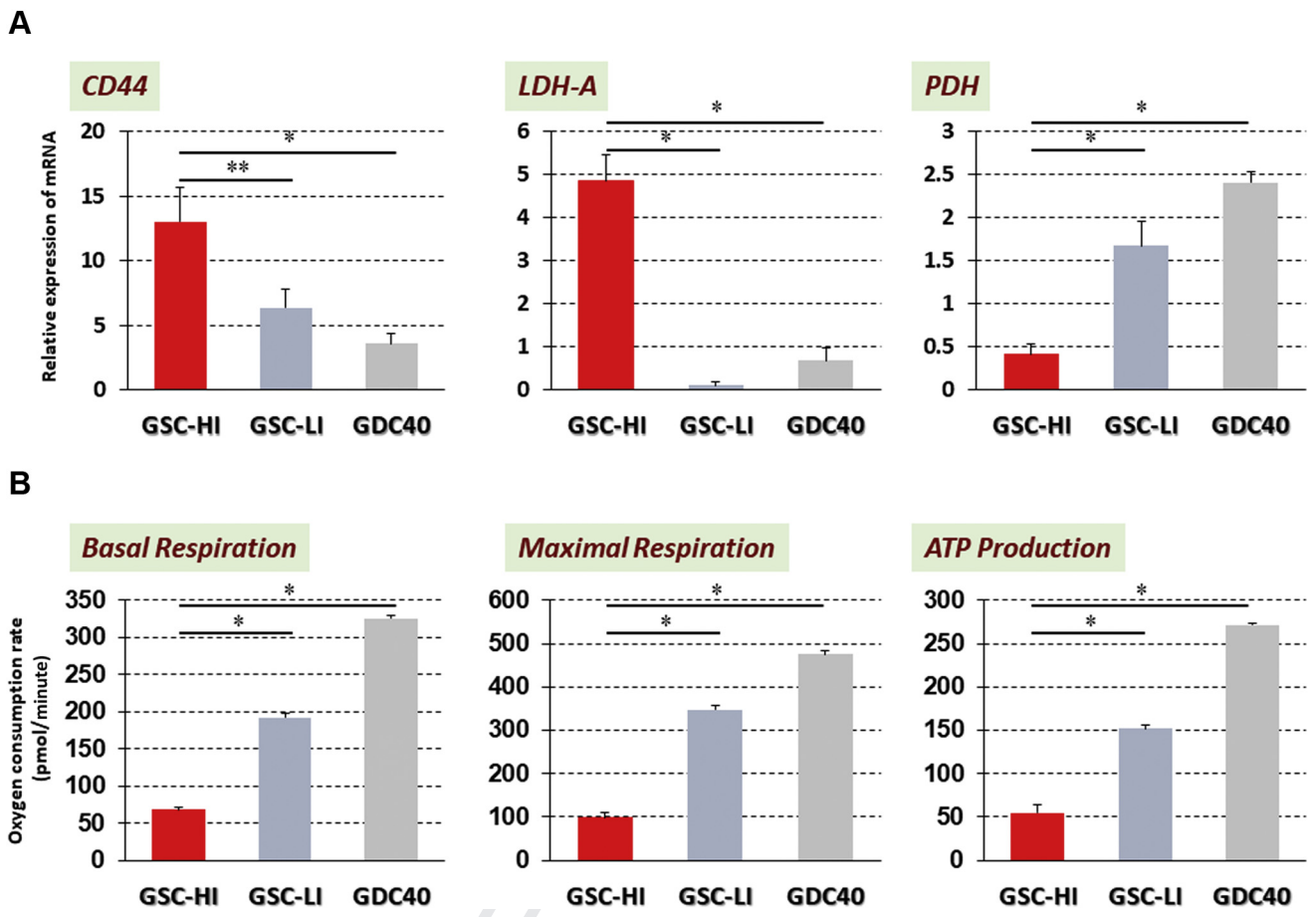

Figure 4. (**A**) Messenger RNA expression of *CD44*, lactate dehydrogenase A (*LDHA*), and pyruvate dehydrogenase (*PDH*) in 3 glioma stemlike cell (GSC) lines. The GSC-HI line (highly invasive) showed the highest level of expression of *CD44* and *LDH-A* and the lowest level of expression of *PDH* among the 3 tested GSC lines (*$P < 0.001$, **$P < 0.01$). (**B**) Cell metabolic rate was measured in the 3 tested GSC lines using an XFp Extracellular Flux Analyzer to assess the oxygen consumption rate (OCR). The OCR was used to evaluate basal respiration, maximal respiration, and adenosine triphosphate (ATP) production. For all 3 indices of mitochondrial function, GSC-HI showed the lowest values among the 3 tested GSC lines (*$P < 0.001$). LI, low-invasive.

factor 1 (HIF-1); the activity of PDH is inhibited by PDH kinase 1 (PDK-1), an enzyme encoded by a gene with a transcription that is also activated by HIF-1α. As a result, measurement of the level of Lac produced by the enzymatic reaction of LDH-A may make it possible to evaluate the degree of hypoxia at the area of interest, specifically in the tumor periphery of GBM.[32-35]

In the present study, 20 patients with GBM were classified into 2 phenotypes, HI and LI, based on their characteristic features on MRI and Met-PET.[3] To elucidate which pathway HI-type and LI-type GBMs favor for glucose metabolism, we investigated mRNA expression, in the tumor periphery of GBMs, of the genes encoding subunits of 2 key enzymes. Because the present study is limited by the relatively small number of patients, a more extensive analysis of a larger patient cohort is required to verify the results. However, we obtained the following results showing significantly high P values.

The qRT-PCR analysis showed that *LDH-A* was expressed at significantly higher levels in HI GBM than in LI GBM, whereas *PDH* was expressed at significantly higher levels in LI GBM than in HI GBM. These expression patterns of the transcripts encoding subunits of 2 key metabolic enzymes likely coincide with hypoxic levels of the tumor periphery in HI-type and LI-type GBMs. That is, the tumor periphery of HI GBM may be more hypoxic than that of LI GBM. Previously, we showed that the P/C ratio of *CD44* mRNA expression permitted differentiation of HI GBM from LI GBM when using a cutoff value of 7.48 for the P/C ratio of *CD44* expression.[3] In addition, severe hypoxia under 1% oxygen has been shown to upregulate the expression of CD44 through HIF-1α.[36] In the present study, 10 of 11 patients with HI GBM showed a P/C ratio for *CD44* expression of >7.8, and the mean P/C ratio of *CD44* expression in HI GBM was significantly higher than that in LI GBM. The *LDH-A* expression in each patient

FLA 5.6.0 DTD ■ WNEU17386_proof ■ 2 July 2021 ■ 8:36 pm ■ ce

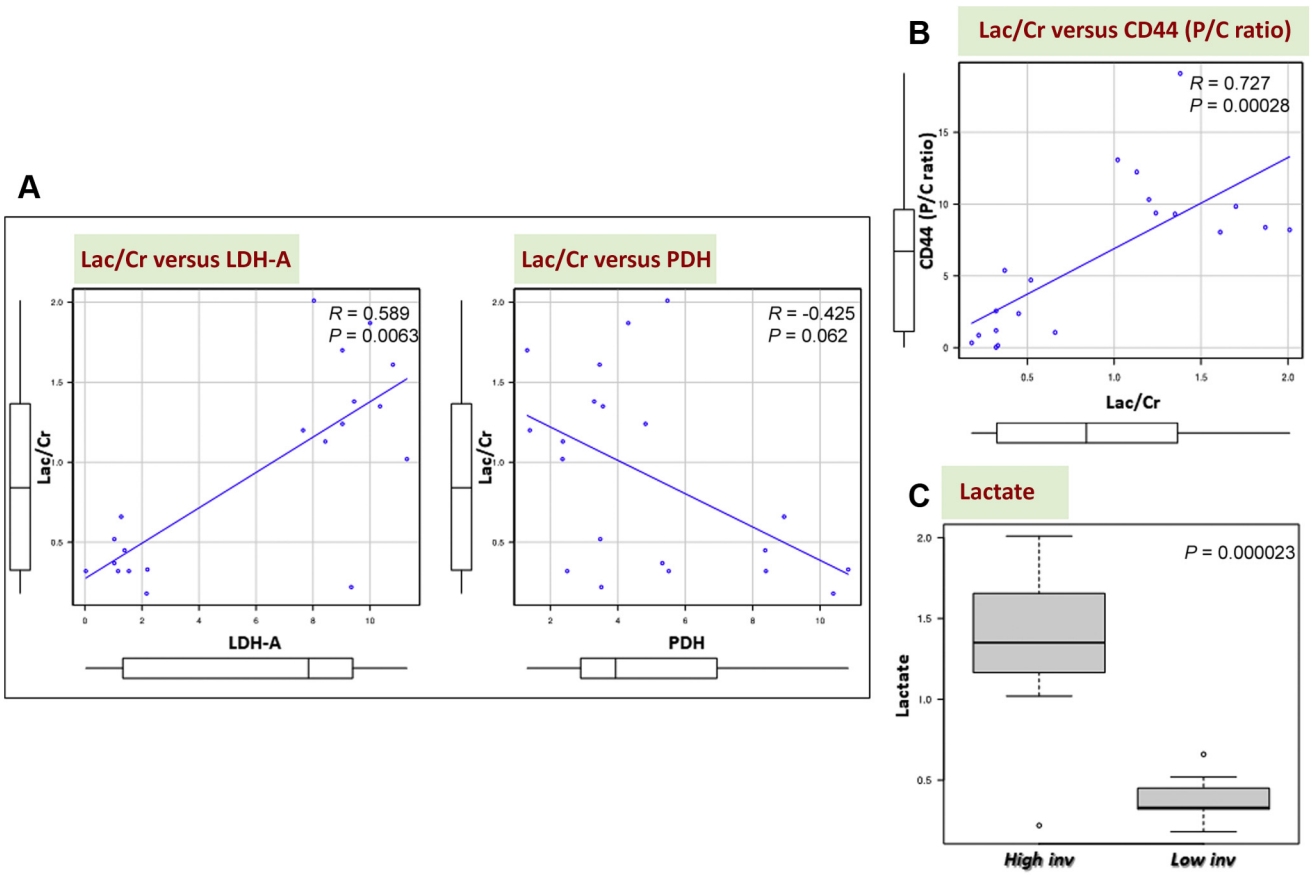

Figure 5. (**A**) The values of the lactate (Lac)/creatine (Cr) ratio (lactate concentration normalized to creatine concentration) showed a significant positive correlation with the level of lactate dehydrogenase A (*LDH-A*) expression in 20 patients with glioblastoma (GBM) ($R = 0.589$; $P = 0.0063$), but showed no significant correlation with the level of pyruvate dehydrogenase (*PDH*) expression ($R = 0.425$; $P = 0.062$). (**B**) The values of the Lac/Cr ratio showed a significant positive correlation with *CD44* expression (ratio of *CD44* transcript level in the tumor periphery to that in the tumor core; periphery/core [P/C] ratio) ($R = 0.727$; $P = 0.00028$). (**C**) Highly invasive (inv) GBM showed significantly higher values of the Lac/Cr ratio than did low-invasive GBM ($P = 0.000023$). The cutoff value for distinguishing high-invasive and low-invasive GBMs was 0.66 (sensitivity, 100%; specificity, 90.9%); values exceeding this cutoff were indicative of high-invasive-type GBM.

showed a significant positive correlation to the value of the P/C ratio of *CD44* expression, whereas *PDH* expression showed a significant negative correlation to the value of the P/C ratio of *CD44* expression. These results support our hypothesis that aerobic glycolysis is used in the tumor periphery of the HI GBM, strongly suggesting that measurement of Lac production by MRS may permit evaluation of the tumor-infiltrating area around the Gd-enhanced tumor mass, providing a technique that might replace Met-PET in this context.

To investigate whether GSCs in the tumor periphery of HI GBM and LI GBM metabolize glucose by different glycolytic pathways, the expression of *LDH-A* and *PDH*, as well as mitochondrial oxygen consumption, were analyzed using 3 GSC lines with distinct invasive activities. A GSC cell line showing high invasiveness and high *CD44* expression (GSC-HI) showed the highest expression of *LDH-A* and the lowest expression of *PDH* among the 3 GSC lines. In addition, the OCR of GSC-HI showed the lowest values in both respiration activities and ATP production compared with the other 2 GSC lines showing low invasiveness and low *CD44* expression. These results indicated that HI tumors predominantly use aerobic glycolysis, whereas LI tumors predominantly use the oxygen-consuming TCA cycle. Accordingly, HI GBM can produce more Lac, resulting in an acidic environment that further enhances the invasive activity of the tumor. Consequently, analysis of the production of Lac may replace *CD44* expression as a marker for tumor invasiveness of GSCs in the tumor periphery of GBM.

To quantitatively analyze the metabolite production on MRS, we used the LC-Model algorithm. This algorithm facilitates the quantitative analysis of metabolites from ^{1}H-MRS.[12,13] The software automatically processes the spectrum of the raw DICOM (Digital Imaging and Communications in Medicine) data obtained by the MRS (e.g., Fourier transform and phase correction), compares the results with the basis-set data for each MRI device and echo time value and automatically calculates the

FLA 5.6.0 DTD ■ WNEU17386_proof ■ 2 July 2021 ■ 8:36 pm ■ ce

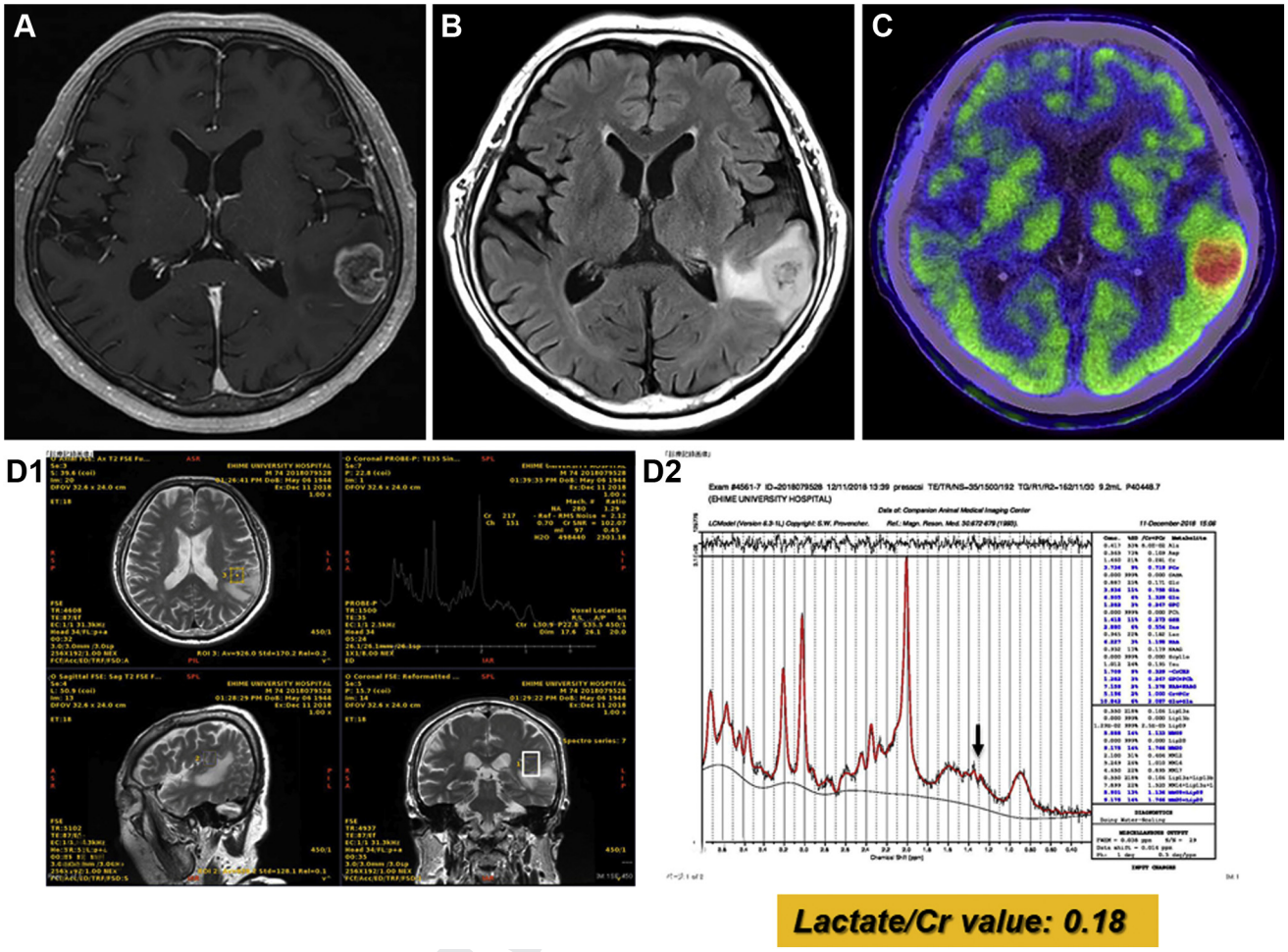

Figure 6. Neuroimaging showing gadolinium (Gd)-enhanced magnetic resonance imaging (MRI), fluid-attenuated inversion recovery (FLAIR), and methionine (Met)-positron emission tomography (PET) of presented case 2. On admission imaging (**A**, T1-Gd; **B**, FLAIR; **C**, Met-PET; **D**, magnetic resonance spectroscopy analysis using the Learning-Compression Model algorithm), Gd-enhanced MRI showed a homogeneously enhanced tumor in the left temporal lobe and perifocal hyperintensity on FLAIR. PET scan showed strongly increased uptake of Met in the left temporal lobe, consistent with the lesion shown on MRI (maximum standard uptake values for Met [tumor/contralateral normal brain tissue ratio], 4.38). On magnetic resonance spectroscopy analysis using the Learning-Compression Model algorithm, the lactate/creatine value was 0.18 in the Met accumulation sites with tumor/contralateral normal brain tissue ratio 1.4 outside the Gd contrast area on MRI (*black arrow*, lactate).

amount of each metabolite from the peak areas obtained by peak separation for each metabolite. In the present study, the amount of Lac, which was calculated using the LC-Model, was presented as a Lac/Cr ratio (i.e., normalized to Cr). In 20 patients with GBM, the Lac/Cr ratio showed a significant positive correlation with level of *LDH-A* expression; no such correlation was observed for *PDH* expression. Furthermore, Lac/Cr ratio values showed a significant positive correlation with the P/C ratio of *CD44* expression. HI GBM had a significantly higher Lac/Cr ratio than did LI GBM. The cutoff for HI GBM was >0.66. In the present study, we found no significant difference in age, Karnofsky Performance Status, MGMT status (as assessed by quantitative methylation-specific PCR after bisulfate modification of genomic DNA), IDH-1 mutational status (as assessed by Sanger sequencing), or Ki-67 staining index (as assessed by immunohistochemistry) between the tumors of HI and LI types. We also detected no significant difference in the extent of resection between GTR and non-GTR (subtotal resection and partial resection). Consequently, the value of Lac/Cr ratio determined by MRS may serve as a novel marker to predict the degree of tumor invasiveness of GBM, in addition to *CD44* expression in the tumor periphery.

On the other hand, the metabolism in astrocytes and neurons, which function synergistically to affect cerebral blood flow and oxygen metabolism,[37] should also be considered when evaluating Lac levels in the extracellular space of the peritumoral area. Astrocytes primarily function using ATP generated by glycolysis,

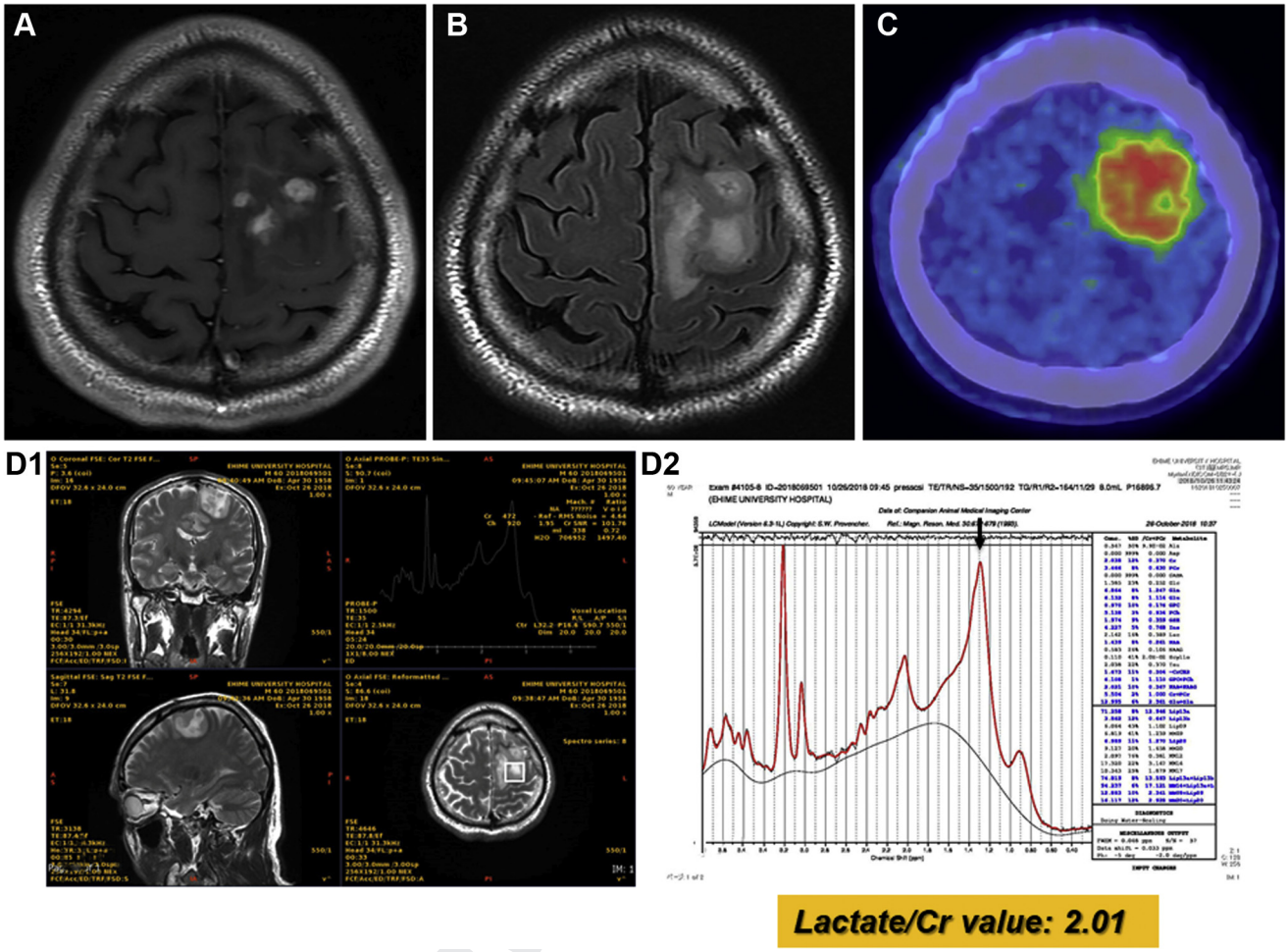

Figure 7. Neuroimaging showing gadolinium (Gd)-enhanced magnetic resonance imaging (MRI) (**A**), fluid-attenuated inversion recovery (FLAIR) (**B**) and methionine (Met)-positron emission tomography (PET) (**C**) on admission of presented case 1. Gd-enhanced MRI showed several enhanced masses in the left frontal lobe and perifocal edema on FLAIR. PET scan showed highly increased uptake of Met in the left temporal lobe, consistent with the lesion shown on MRI (maximum standard uptake values for Met [tumor/contralateral normal brain tissue ratio], 5.21). On magnetic resonance spectroscopy analysis using the Learning-Compression Model algorithm, the lactate/creatine value was 2.01 in the Met accumulation sites with tumor/contralateral normal brain tissue ratio 1.4 outside the Gd contrast area on MRI (*black arrow*, lactate) (**D**).

releasing high levels of Lac. This extracellular Lac is transported to neurons for aerobic metabolism to obtain large amounts of energy. In the present study, measurement of NAA on MRS, representing the existence of neurons, showed that NAA/Cr correlated negatively with Lac/Cr (**Supplementary Figure 3**) and that HI-type GBMs presented lower values for NAA/Cr than did LI-type GBMs. These results suggest that many more neurons may be lost in HI-type GBMs and that astrocytes can promote tumor cell invasion by enhancing the acidity of the microenvironment at the periphery of GBM. In contrast, no correlations were evident between glutamate and Lac or between Gln and Lac. Astrocytes function to maintain neurotransmitter stores via the Gln-glutamate cycle.[38] Glutamate released from neurons is rapidly taken up by astrocytes and converted to Gln, which is then re-released into the extracellular space for neuronal re-uptake and subsequent generation of glutamate. In this cycle, uptake of glutamate by astrocytes promotes glucose metabolism from oxidative phosphorylation via the TCA cycle to aerobic glycolysis in astrocytes, resulting in greater production of Lac.[39] Because significantly fewer neurons were present around HI-type GBMs than around LI-type GBMs, levels of Gln might be expected to be higher in HI-type GBMs than in LI-type GBMs. However, the present data did not show significant correlations between Gln/Cr and high tumor invasiveness (**Supplementary Figure 4**).

When the tumor infiltration area including GSCs is identified preoperatively solely by the amount of Lac evaluated on MRS, it will be valuable to know (at a gross level) the extent of the tumor infiltration area around the Gd-enhanced tumor mass; this

FLA 5.6.0 DTD ■ WNEU17386_proof ■ 2 July 2021 ■ 8:36 pm ■ ce

knowledge will facilitate obtaining tissue from appropriate sites for the measurement of Lac level on MRS. Previously, we reported that most GBMs in the tumor infiltration area of the tumor periphery existed within 30 mm of the border of the Gd-enhanced tumor mass.[6] This observation suggests that the target sites for measuring Lac on MRS should include the areas within 30 mm of the main tumor border. As future work allowing more effective application of the present results to clinical practice, we plan to study MRS mapping of Lac and NAA concentrations in the tumor-infiltrating area outside the Gd-enhanced tumor mass in GBM, which should provide crucial information for the treatment of GBM.

CONCLUSIONS

The gene encoding a subunit of *LDH-A* was expressed at a significantly higher level in HI-type GBM showing high *CD44* expression than in LI-type GBM showing low *CD44* expression in the tumor periphery of GBM. In contrast, *PDH* was expressed at a higher level in LI GBM than in HI GBM. In addition, a GSC line (GSC-HI) showing high invasiveness and high *CD44* expression showed the highest *LDH-A* expression and the lowest *PDH* expression among 3 GSC lines. Furthermore, GSC-HI showed the lowest level of oxygen consumption and ATP production. Lac measured on MRS using the LC-Model algorithm (expressed as the Lac/Cr ratio) showed a significant positive correlation with the level of *LDH-A* transcript, but not with that of PDH, in 20 patients with GBM. Patients with HI GBM showed higher Lac/Cr ratios than did those with LI GBM; this comparison showed a cutoff value of 0.66. These results indicated that HI GBMs (with GSCs in the tumor periphery) metabolize glucose predominantly via aerobic glycolysis, resulting in the production of Lac; thus, the quantitative measurement of Lac production on MRS may serve as a useful marker for prediction of GBM invasiveness and identification (proximal to the Gd-enhanced tumor mass) of the GSC-infiltrated area lacking Gd enhancement. This finding may lead to enhanced therapeutic planning, improving the clinical prognosis for GBM.

CRediT AUTHORSHIP CONTRIBUTION STATEMENT

Akihiro Inoue: Conceptualization, Formal analysis, Data curation, Writing - original draft. **Masahiro Nishikawa:** Conceptualization, Formal analysis, Data curation, Writing - review & editing. **Takanori Ohnishi:** Conceptualization, Formal analysis, Writing - review & editing. **Hajime Yano:** Data curation. **Yonehiro Kanemura:** Data curation, Writing - review & editing. **Yoshihiro Ohtsuka:** Data curation. **Saya Ozaki:** Data curation. **Yawara Nakamura:** Data curation. **Shirabe Matsumoto:** Data curation. **Satoshi Suehiro:** Writing - review & editing. **Daisuke Yamashita:** Writing - review & editing. **Seiji Shigekawa:** Writing - review & editing. **Hideaki Watanabe:** Writing - review & editing, Supervision. **Riko Kitazawa:** Data curation. **Junya Tanaka:** Writing - review & editing, Supervision. **Takeharu Kunieda:** Writing - review & editing, Supervision.

ACKNOWLEDGMENTS

The authors express their gratitude to Taichi Furumochi and Yasuhiro Shiraishi of the Department of Neurology, Ehime University Hospital, Japan; and to Satsuki Myoga of the Department of Pathology, Ehime University Hospital, Japan, for their help in obtaining pathologic and radiologic image findings. We also thank Kohei Miura and Koji Maehara at GE Healthcare Japan for their advice regarding the technical background of MRS sequences and the postprocessing steps during the revision process.

REFERENCES

1. Stupp R, Mason WP, van den Bent MJ, et al. Radiotherapy plus concomitant and adjuvant temozolomide for glioblastoma. *N Engl J Med*. 2005;352:987-996.

2. Stupp R, Hegi ME, Mason WP, et al. Effects of radiotherapy with concomitant and adjuvant temozolomide versus radiotherapy alone on survival in glioblastoma in a randomized phase III study: 5-year analysis of the EORTC-NCIC trial. *Lancet Oncol*. 2009;10:459-466.

3. Nishikawa M, Inoue A, Ohnishi T, et al. Significance of glioma stem-like cells in the tumor periphery that express high levels of CD44 in tumor Invasion, early progression, and poor prognosis in glioblastoma. *Stem Cells Int*. 2018;23:5387041.

4. Jacobs AH, Winkler A, Dittmar C, et al. Molecular and functional imaging technology for the development of efficient treatment strategies for gliomas. *Technol Cancer Res Treat*. 2002;1:187-204.

5. Galldiks N, Ullrich R, Schroeter M, et al. Volumetry of [(11)C]-methionine PET uptake and MRI contrast enhancement in patients with recurrent glioblastoma multiforme. *Eur J Nucl Med Mol Imaging*. 2010;37:84-92.

6. Inoue A, Ohnishi T, Kohno S, et al. Met-PET uptake index for total tumor resection: identification of 11C-methionine uptake index as a goal for total tumor resection including infiltrating tumor cells in glioblastoma. *Neurosurg Rev*. 2021; 44:587-597.

7. Warburg O. The metabolism of carcinoma cells. *J Cancer Res*. 1925;9:148-163.

8. Warburg O. On the origin of cancer cells. *Science*. 1956;123:309-314.

9. Pellerin L, Magistretti PJ. Glutamate uptake into astrocytes stimulates aerobic glycolysis: a mechanism coupling neuronal activity to glucose utilization. *Proc Natl Acad Sci U S A*. 1994;91: 10625-10629.

10. Magistretti PJ, Pellerin L, Rothman DL, et al. Energy on demand. *Science*. 1999;283:496-497.

11. Kasischke KA, Vishwasrao HD, Fisher PJ, et al. Neural activity triggers neuronal oxidative metabolism followed by astrocytic glycolysis. *Science*. 2004;305:99-103.

12. Choi C, Ganji SK, DeBerardinis RJ, et al. 2-hydroxyglutarate detection by magnetic resonance spectroscopy in IDH-mutated patients with gliomas. *Nat Med*. 2012;18:624-629.

13. Pope WB, Prins RM, Albert Thomas M, et al. Non-invasive detection of 2-hydroxyglutarate and other metabolites in IDH1 mutant glioma patients using magnetic resonance spectroscopy. *J Neurooncol*. 2012;107:197-205.

14. Andronesi OC, Rapalino O, Gerstner E, et al. Detection of oncogenic IDH1 mutations using magnetic resonance spectroscopy of 2-hydroxyglutarate. *J Clin Invest*. 2013;123:3659-3663.

15. Kanemura Y, Mori H, Kobayashi S, et al. Evaluation of in vitro proliferative activity of human fetal neural stem/progenitor cells using indirect measurements of viable cells based on cellular metabolic activity. *J Neurosci Res*. 2002;69:869-879.

16. Nishikawa M, Inoue A, Ohnishi T, et al. CD44 expression in the tumor periphery predicts the responsiveness to bevacizumab in the treatment of recurrent glioblastoma. *Cancer Med*. 2021;10: 2013-2025.

17. Bamba Y, Shofuda T, Kanematsu D, et al. Differentiation, polarization, and migration of human induced pluripotent stem cell-derived neural progenitor cells co-cultured with a human glial cell line with radial glial-like characteristics. *Biochem Biophys Res Commun*. 2014;447:683-688.

18. Banh RS, Iorio C, Marcotte R, et al. PTP1B controls non-mitochondrial oxygen consumption by regulating RNF213 to promote tumour survival during hypoxia. *Nat Cell Biol*. 2016;18:803-813.

19. Garaude J, Acín-Pérez R, Martínez-Cano S, et al. Mitochondrial respiratory-chain adaptations in macrophages contribute to antibacterial host defense. *Nat Immunol*. 2016;17:1037-1045.

20. Bottomley PA. Spatial localization in NMR spectroscopy in vivo. *Ann N Y Acad Sci*. 1987;508:333-348.

21. Ogg RJ, Kingsley PB, Taylor JS. WET, a T1- and B1-insensitive water-suppression method for in vivo localized 1H NMR spectroscopy. *J Magn Reson B*. 1994;104:1-10.

22. Provencher SW. Estimation of metabolite concentrations from localized in vivo proton NMR spectra. *Magn Reson Med*. 1993;30:672-679.

23. Smith SA, Levante TO, Meier BH, et al. Computer simulations in magnetic resonance. An object oriented programming approach. *J Magn Reson*. 1994;106:75-105.

24. Kanda Y. Investigation of the freely available easy-to-use software 'EZR' for medical statistics. *Bone Marrow Transpl*. 2013;48:452-458.

25. Ohue S, Kohno S, Inoue A, et al. Surgical results of tumor resection using tractography-integrated navigation-guided fence-post catheter techniques and motor-evoked potentials for preservation of motor function in patients with glioblastomas near the pyramidal tracts. *Neurosurg Rev*. 2015;38:293-306.

26. Okita Y, Nonaka M, Shofuda T, et al. 11)C-methinine uptake correlates with MGMT promoter methylation in nonenhancing gliomas. *Clin Neurol Neurosurg*. 2014;125:212-216.

27. Li YM, Suki D, Hess K, et al. The influence of maximum safe resection of glioblastoma on survival in 1229 patients: can we do better than gross-total resection? *J Neurosurg*. 2016;124:977-988.

28. Pessina F, Navarria P, Cozzi L, et al. Maximize surgical resection beyond contrast-enhancing boundaries in newly diagnosed glioblastoma multiforme: is it useful and safe? A single institution retrospective experience. *J Neurooncol*. 2017;135:129-139.

29. Ohnishi T. Recent progress in surgery of malignant gliomas in and near eloquent cortical areas. *Prog Neuro-Oncology*. 2014;21:1-13.

30. Lasocki A, Gaillard F, Tacey M, et al. Incidence and prognostic significance of non-enhancing cortical signal abnormality in glioblastoma. *J Med Imaging Radiat Oncol*. 2016;60:66-73.

31. Lasocki A, Gaillard F. Non-contrast-enhancing tumor: a new frontier in glioblastoma research. *AJNR Am J Neuroradiol*. 2019;40:758-765.

32. Tang C, Liu W. LDHA is a feedback activator of hypoxia inducible factor 1-alpha in ovarian cancer. *Int J Clin Exp Pathol*. 2016;9:10437-10443.

33. Serganova I, Cohen IJ, Vemuri K, et al. LDH-A regulates the tumor microenvironment via HIF-signaling and modulates the immune response. *PLoS One*. 2018;13:e0203965.

34. Kim JW, Tchernyshyov I, Semenza GL, et al. HIF-1-mediated expression of pyruvate dehydrogenase kinase: a metabolic switch required for cellular adaptation to hypoxia. *Cell Metab*. 2006;3:177-185.

35. Dang CV, Semenza GI. Oncogenic alterations of metabolism. *Trends Biochem Sci*. 1999;24:68-72.

36. Nishikawa M, Inoue A, Ohnishi T, et al. Hypoxia-induced phenotypic transition from highly invasive to less invasive tumors in glioma stem-like cells: significance of CD44 and osteopontin as therapeutic targets in glioblastoma. *Trans Oncol*. 2021;14:101137.

37. Deitmer JW, Theparambil SM, Ruminot I, et al. Energy dynamics in the brain: contributions of astrocytes to metabolism and pH homeostasis. *Front Neurosci*. 2019;13:1301.

38. Bergles DE, Jahr CE. Synaptic activation of glutamate transporters in hippocampal astrocytes. *Neuron*. 1997;19:1297-1308.

39. Watts ME, Pocock R, Claudianos C. Brain energy and oxygen metabolism: emerging role in normal function and disease. *Front Mol Neurosci*. 2018;11:216.

Received 21 March 2021; accepted 7 June 2021

Citation: World Neurosurg. (2021). https://doi.org/10.1016/j.wneu.2021.06.044

*Journal homepage: **www.journals.elsevier.com/world-neurosurgery***

*Available online: **www.sciencedirect.com***

APPENDIX

1) Image-guided navigation surgery and selective tissue sampling

Tumor resection was performed by echo-linked navigation-guided surgery using magnetic resonance imaging (MRI) and methionine (Met)-positron emission tomography (PET) fusion images and fence-post catheter techniques. Tumor tissue sampling was performed by obtaining the area of maximum standard uptake value (SUV_{max}) on Met-PET and defining areas with positive ^{11}C-Met uptake but no gadolinium (Gd) enhancement at the tumor periphery.

1) MRI and Met-PET

MRI was performed using a 3-T scanner and axial, coronal, and sagittal T1-weighted images with and without Gd contrast enhancement were obtained with slice thickness of 2 mm. ^{11}C-Met-PET data were acquired and the SUV_{max} was calculated from the pixel values of a region of interest with reference to the tumor image on Gd-enhanced MRI. The tumor/contralateral normal brain tissue ratio (TNR) was determined by dividing the tumor SUV_{max} by the mean standard uptake value of the contralateral occipital lobe.

3) Glioma stemlike cell culture

Glioma stemlike cells were obtained from the primary cell culture of tumor tissues at the periphery of the glioblastoma multiforme and cultured in serum-free neural stem cell medium. Stemness was confirmed by 10% fetal calf serum–induced multilineage differentiation, high tumorigenicity in the brains of immunodeficient mice, and expression of stem cell markers including CD133 and Nestin.

4) Measurement of mitochondrial energy metabolism

Oxygen consumption rate (OCR) was measured using an XFp Extracellular Flux Analyzer. OCR includes basal respiration, maximal respiration, and adenosine triphosphate (ATP) production as mitochondrial functions.

5) Magnetic resonance spectroscopy (MRS)

The magnetic resonance spectral data were acquired using a 3-T-MRI/MRS scanner. Single-voxel localized magnetic resonance spectra were acquired using the double-echo point-resolved spectroscopy sequence. Voxels were localized to representative areas of solid tumor and regions including necrosis, hemorrhage, or cystic changes were excluded from the interrogated area.

6) Learning-Compression (LC) Model algorithm

To quantitatively evaluate the concentrations of various metabolites on MRS, the LC-Model algorithm was introduced. By applying the LC-Model to the magnetic resonance spectral data, the concentration (resonance area ratio; mmol/L) of each molecule, including 2-hydroxyglutarate, glutamate, glutamine, choline, creatine, N-acetyl-aspartate, and lactate, was calculated at any 3 points in the Met-uptake area at TNR 1.4 outside Gd-enhanced tumor mass. The calculated concentrations of these metabolites were presented as ratios of each metabolite concentration to creatine concentration, in units of relative millimoles per liter (when creatine is set to 1.0).

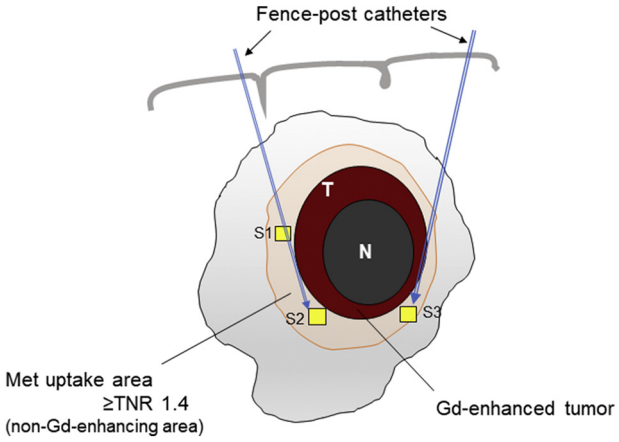

Supplementary Figure 1. Technical procedures for obtaining tumor tissue samples from the border area between the gadolinium (Gd)-enhanced tumor mass and surrounding brain tissue. Fence-post catheters are placed along the enhancing tumor border under an echo-linked image-guided navigation system and the tips of the catheters are set as targets (*S2*, *S3*) to obtain samples from the periphery. A tumor sample at another target (*S1*) is obtained from about the midpoint on the pathway between catheters. Sampling from the tumor core is generally obtained from the area showing maximum standard uptake value on methionine (Met)-positron emission tomography. TNR, tumor/contralateral normal brain tissue ratio.

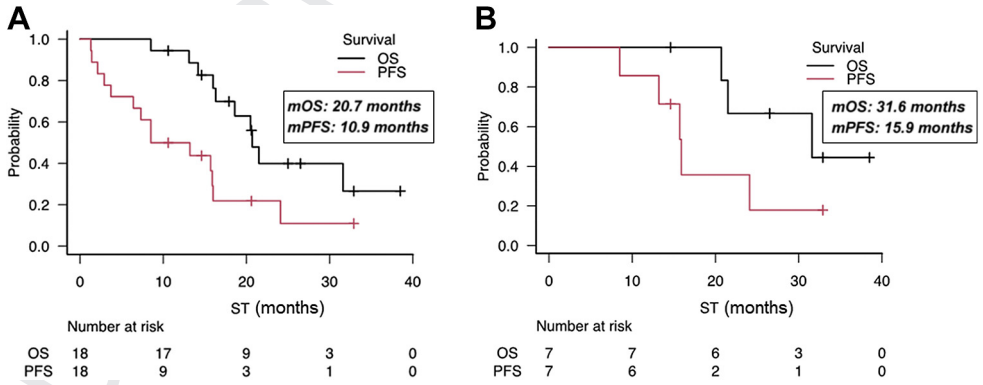

Supplementary Figure 2. Kaplan-Meier survival curves of overall survival (OS) and progression-free survival (PFS) in (**A**) all 18 patients except 2 patients, in whom follow-up periods are very short, and (**B**) in 7 patients who received extensive total resection of tumors (ETR) with infiltrating tumor cells around the gadolinium (Gd)-enhanced tumor mass. Median OS (mOS) and PFS (mPFS) in 18 patients were 20.7 months and 10.85 months, respectively, and those in 7 patients with ETR were 31.6 months and 15.9 months, respectively. Because the patients with ETR were included in all patients, statistical difference in the survival times (STs) between these 2 groups was not obtained.

FLA 5.6.0 DTD ■ WNEU17386_proof ■ 2 July 2021 ■ 8:36 pm ■ ce

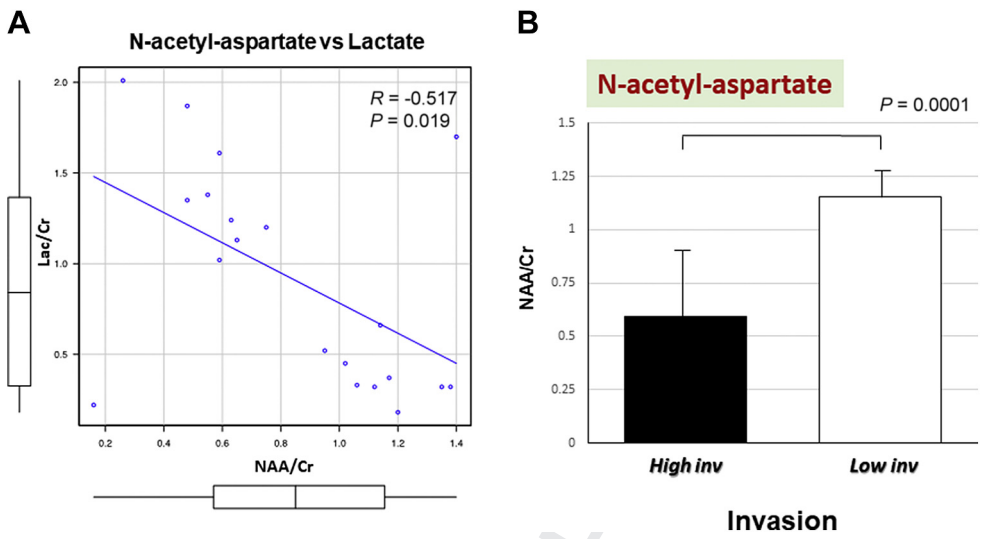

Supplementary Figure 3. (**A**) *N*-acetyl-aspartate (NAA)/creatine (Cr) ratio (NAA concentration normalized to Cr concentration) shows a significant negative correlation with lactate (Lac)/Cr ratio in 20 patients with glioblastoma (GBM) ($R = -0.517$; $P = 0.019$). (**B**) Highly invasive (inv) GBM shows significantly lower NAA/Cr ratio than low-invasive GBM ($P = 0.0001$).

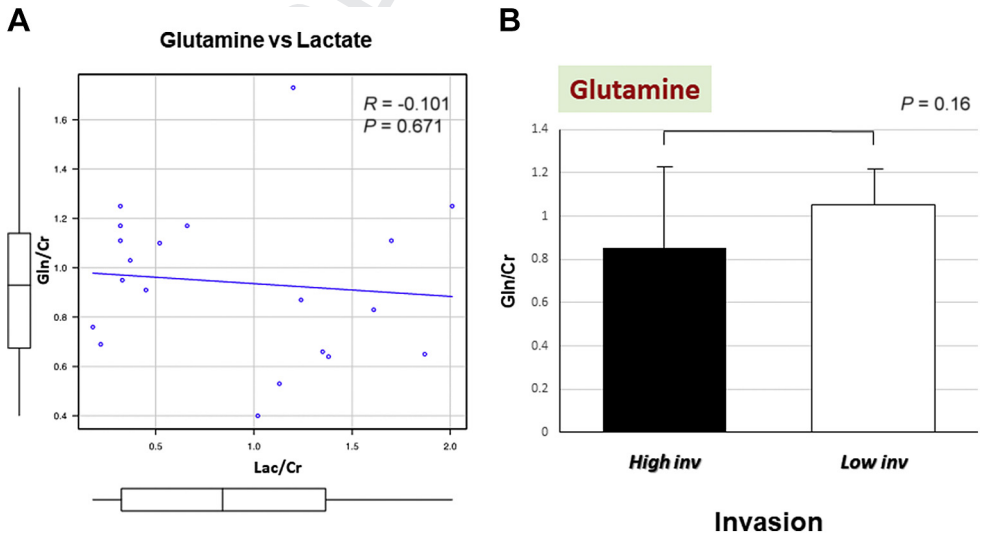

Supplementary Figure 4. (**A**) Glutamine (Gln)/creatine (Cr) ratio (glutamine concentration normalized to creatine concentration) shows no significant correlation with lactate (Lac)/Cr ratio in 20 patients with glioblastoma (GBM) ($R = -0.101$; $P = 0.671$). (**B**) Highly invasive (inv) GBM and low-invasive GBM do not show significant differences in Gln/Cr ratio ($P = 0.16$).

FLA 5.6.0 DTD ■ WNEU17386_proof ■ 2 July 2021 ■ 8:36 pm ■ ce

Supplementary Table 1. Oligonucleotide Primers Used for Quantitative Real-Time Reverse Transcription-Polymerase Chain Reaction

Gene	Sense/Antisense
CD44	5′-AGAAGGTGTGGGCAGAAGAA-3′
	5′-AAATGCACCATTTCCTGAGA-3′
LDH-A	5′-TGAAGGGAGGAGATGATGGAT-3′
	5′-ACGCTGGACCAAATTAAGAC-3′
PDH	5′-AGCTGGGCTACCACATCTAC-3′
	5′-CATTGACTGGGTTTTCTTCC-3′
GAPDH	5′-CAGTCAGCCGCATCTTCTTT-3′
	5′-TGACGGTGCCATGGAATTTG-3′

FLA 5.6.0 DTD ■ WNEU17386_proof ■ 2 July 2021 ■ 8:36 pm ■ ce